

THESIS FOR THE DEGREE OF LICENTIATE OF ENGINEERING

# **New Nanopores for Combined Plasmonic and Electrical Sensing**

Kunli Xiong



Department of Applied physics  
CHALMERS UNIVERSITY OF TECHNOLOGY  
Göteborg, Sweden 201

# **New Nanopores for Combined Plasmonic and Electrical Sensing**

KUNLI XIONG

KUNLI XIONG, 2016

Licentiate Thesis at Chalmers University of Technology

Department of Energy and Environment

SE-412 96 Göteborg

Sweden

Telephone +46(0)72-9371508

Cover:

Applications based on functional nanopores

Chalmers Bibliotek, Reproservice

Göteborg, Sweden 2016

New nanopores for Combine Plasmonic and Electrical Sensing

Kunli Xiong

Department of Energy and Environment

Chalmers University of Technology

## **Abstract**

In this thesis, several kinds of artificial plasmonic biosensors are introduced. They have different nanostructures which are nanoholes, nanowells and nanopores. The fabrication technologies are introduced. All these nanostructures are fabricated based on colloidal lithography technology and following by several special steps. Different kinds of nanostructures can be used for different purposes, nanoholes is one of the simplest biosensors, which can be used to detect one kind of targets. Nanowells has different plasmonic signals for different binding positions. Nanopores can act not only as a biosensor but also nanofluidics.

All these plasmonic biosensors have plasmonic signals, which provide the information for sensing. Depending on observing the shifts of the peak and the dip for plasmonic signal, the reaction between the targets and the receptors on the sensor surface can be detected. The theoretical analyzing and mathematic functions of plasmonic signals are introduced. For different nanostructures, the plasmonic signals are also different. Even for the same kind of nanostructures, the position of the peak and the dip are also influenced by the periodicity, the diameters of the nanostructures and the thickness of metal layer.

The plasmonic biosensors could have lots of additional applications after combing other technologies, the plasmonic thermal sensor is one of them. This special sensor is produced by implementing the electrical technology on nanoholes sample. After applying electronic currents, the nanoholes sample can produce thermal energy, meanwhile, it can also provide plasmonic signals. By calculation the resistance of the metal film, the temperature can be gotten, so the plasmonic biosensor can be used to heat targets with specific temperature and also observe the surface condition of the biosensor based on the variation of the plasmonic signal.

Index Terms: Plasmonic, Biosensor, Colloidal lithography, Surface, Electrical technology, Thermal Energy.

## Acknowledgements

I would like to express my sincere gratitude to Prof. Andreas B. Dahlin, for employing me to start my PHD life in Chalmers. As the supervisor of my project, he always supports and encourages me during the research. He patiently teaches me and cares for my life like a brother. It is very lucky to work for him. I would also like to thank my co-supervisor, Prof. Edwin Jager. Even he is not working in Chalmers instead of Linköping university, he is still carefully teaching and supporting me with useful information. I learned the deposition polymer technologies directly from him, which is a quite important part for my project. Thanks a lot for my examiner Prof. Mikeal Käll and project reviewer Prof. Jie Sun, they help and discuss a lot for my licentiate thesis.

Many thanks as well to my colleagues Gustav Emilsson, who helps me to finish lots of chemistry experiments and we always discuss plans in the daily research. Lei Shao is also one of the best advisers, I always can get some new ideas from our discussion. Yurui Wang as a postdoc teaches me lots of theoretical knowledge and software technologies. Martin Wersäll shares the office with me, he always helps me both on research and daily life. He lets me know lots of Swedish cultures and friendly invites me to join some activities. Ruggero Verre and Srdjan Acimovic who are experienced researchers, they always help me with fabrication samples and give lots of useful advice.

Then, I would like to thank two postdoc friends, Zhaoyang Zhang and Lihui Liu. Both of them are from Jie Sun group. We always play together and discuss academic problems during the lunch time. They have rich physics and electrochemistry knowledge, they always help me to find useful experimental materials and equipments, encourage me when I have troubles.

To my family: First, I want to say I am the luckiest man in the world to get married with my wife Zi Yang. She always encourages me and warms my heart. She is one of the biggest sources of energy to push me working hard. 谢谢你老婆! I also want to thank my parents to support me working abroad. They always care of my health and research by internet communication software.

Finally, I want to thank Sweden, which is an equal, free and merciful country! Friendly people, nice environment and good English pronunciation. Hopefully the weather could be better in the future.

^\_^

Kunli Xiong

Göteborg, Sweden

January 10<sup>th</sup>, 2016.

## APPENDEND PAPERS

The following papers are included in the thesis:

Paper I:

*A thermal plasmonic sensor platform: Resistive heating of nanohole arrays*

**K. Xiong** & M. Virk, M. Svedendahl, M. Käll, and A.B. Dahlin.

*Nano Letters* **2014**, 14 (6), 3544-3549.

Paper II:

*Biosensing Using Plasmonic Nanohole Arrays with Small, Homogenous and Tunable Aperture Diameters*

**K. Xiong**, G. Emilsson and A.B. Dahlin.

*Sumbmitted* **2016**.

Paper III:

*Plasmonic Nanopores in Metal-Insulator-Metal Films*

A. B. Dahlin, M. Mapar, **K. Xiong**, F. Mazzotta, F. Höök, and T. Sannomiya.

*Adv. Opt. Mater* **2014**, 2 (6), 556–564.

My main contributions:

I made the simulations for all the models in these papers by COMSOL Multiphysics® Modeling Software. In paper I, I did parts of the measurement like surface temperature, IV curve and plasmonic signals. I also did the polymer absorbing and disrobing experiments. In paper II, I fabricated the samples, measured the plasmonic signals and surveyed SEM images. In paper III, I also did the spectrum measurement and surveyed SEM images.

# Contents

<b>1 Introduction</b>	<b>1</b>
<b>2 Fabrication of nanomaterials</b>	<b>3</b>
2.1 Fabrication of nanoholes	4
2.2 Fabrication of nanowells	7
2.3 Fabrication of nanopores	9
<b>3. Plasmonic properties</b>	<b>13</b>
3.1 Plasmonic signal of nanoholes	13
3.2 Plasmonic signal of nanowells	19
3.3 Plasmonic signal of nanopores	20
<b>4. Implementing electronic techniques</b>	<b>23</b>
<b>5. Summary and Outlook</b>	<b>27</b>

# Chapter 1

## Introduction

Biosensors have a very long history in human society. One of the oldest biosensor is the canary bird, which was used several hundred years ago [1]. Canary birds are quite sensitive to carbon monoxide. The dangerous gas can kill the Canary birds before humans, which could be used to warn the miners to vacate the mine. Nowadays, humans are still using special animals as biosensors, the most common example is the police dog. The olfactory of dogs is several orders of magnitude more sensitive than for humans and dogs can recognize each other by smell. So the dogs can be trained to remember the smell of a target and track it by following the smell. The animal biosensors are widely used all over the world because they are easy to find. However, they are not very reliable and limited by their own organs. For example, canary birds can only detect low amounts of toxic gases. If the amount is too high, both of the human and the birds can die quite fast. Similarly, dogs could be disturbed by other smells, which would mess up their olfactories.

For getting better biosensors, artificial biosensors have been researched several decades [2]. Some of them have already been widely used in daily lives such as the glucose sensor [3], pregnancy sensor [4] and virus sensor [5, 6]. The most successful artificial biosensor is the glucose sensor, which can be used to detect the glucose concentration in human blood. The principle is utilizing the enzyme glucose oxidase to specifically capture and oxidise glucose. The capture and oxidizing induces an electrical current and the glucose concentration in blood can be calculated from the current value. This glucose sensor is quite stable, sensitive and fast. One drop of blood is sufficient for analysis and the whole process just needs a few seconds. During recent years, biosensors have become more and more sensitive due to the development of nanotechnology. Some special sensors utilizing electrochemistry can even detect single molecules [7] and the sequence of DNA [8].

However, lots of artificial biosensors are still hard to use in daily life. One of the biggest problems is that they are too expensive. Research on cheaper raw materials could help to decrease the cost [9] and investigating cheaper fabrication technologies is also a good way. In the last ten years, a new kind of nanofabrication technology called colloidal lithography (CL) has improved [10]. Comparing with other nanofabrication methods such as electron beam lithography (EBL) [11], CL is much more convenient and cheaper. EBL utilizes the electron

beam to write nanopatterns in a photoresist first. Then, the photoresist is developed and the materials are deposited. After washing away the remaining photoresist, the nanostructures are ready. One disadvantage of EBL is that the writing is limited by the electron beam writing speed. EBL can only be used to produce micrometer level sensors. Colloidal lithography utilizes plastic nanoparticles to make nanostructures instead of using electron beams to write nanopatterns one by one. Each particle can form one nanostructure, the sample can absorb billions of particles in a few minutes, so billions of nanostructures can be produced quite fast [12]. In addition, the cost of CL is much less than for EBL because it does not need any special machine to create the vacuum environment and the electron beam. CL seems to have better commercial potential than EBL.

In recent years, the biosensors which make use of optical signals for detection got a huge improvement [13, 14, 15]. Comparing with traditional electrical signals [16, 17], optical biosensors do not need conductive solution to form a closed circuit, which could avoid lots of noise associated with the liquid. The optical biosensors sometimes utilize nanostructured arrays to create one kind of special optical signal which is called a plasmonic signal. Plasmonic signals are very sensitive to the surface condition of the nanostructures. It can be used to detect if the targets bind on the surface or not.

Plasmonic signals are formed by electron oscillations at the interface between metal and dielectric layers [18, 19]. The electron oscillation is quite dependant on the geometry of the nanostructure. This thesis mainly focuses on three kinds of structures. These are nanoholes [20], nanowells [21] and nanopores [22]. They have similar plasmonic signals, which contain two important parts. One part is the peak of the extinction spectrum and the other is the dip of the extinction spectrum. They are formed by different coupling conditions between incident light and the geometry of the structure. Both of them are quite sensitive to the surface condition of the nanostructures. They have clear wavelength shifts when the targets bind on the surface because it changes the refractive index (RI) at the surface. Based on this phenomenon, plasmonic sensors can be used to detect if the targets exist in the liquid or not by attaching the receptors on the surface which capture the targets.

Except the optical properties, the materials of plasmonic biosensors are also quite interesting in other ways. In general, plasmonic biosensors are made of metals and dielectrics, which have quite different electrical properties. Metals are quite good for heating because of high thermal conductivity. Thermal energy can be directly produced by applying a voltage on a metal surface [23]. Plasmonic biosensors often have tens of nanometers thick metal layers. The temperature can reach to several hundred degrees by less than 1 A current, which means that the plasmonic biosensor can also be used as hot plate to provide thermal energy. In addition, plasmonic biosensors could also be used to detect the temperature, because a variation in temperature would change the electron oscillation state, which would lead to shifts in both peak and dip wavelengths.

This thesis contains four chapters. Chapter 2 describes the fabrication technologies of plasmonic biosensors. Three different structures are introduced. They are nanoholes, nanowells and nanopores. Chapter 3 focuses on the theoretical analysis of plasmonic properties. It continues to focus on the three different kinds of biosensor structures, analyse the physical principles and mathematic functions of plasmonic signals. Chapter 3 mainly describes the electrical heating technology. After combining the plasmonic sensor with electrical technology, the biosensor can not only be used to detect plasmonic signals but also to heat bound targets. In Chapter 4, a short summary will be given and some future work will also be presented.

# Chapter 2

## 2. Fabrication of nanomaterials

There is no doubt that the development of fabrication technology for nanomaterials pushes up the modern plasmonic research. During the last decades, the accuracy and versatility of nanofabrication got a huge progress [24]. Electron beam lithography (EBL) which is one of the most popular nanofabrication methods can be used to produce structures on the order of tens of nanometres. Recently, by using the electron beam of transmission electron microscope (TEM) [25], few nanometers nanochannels can also be fabricated. Compared with optical lithography, electron beam is not limited by diffraction phenomenon. For both photolithography and laser lithography, the diffractive phenomenon would limit the size of the light beam, which can decide the precision of written patterns. However, EBL also has some disadvantages compared with photolithography. One disadvantage is that the cost of fabrication nanostructures by EBL is much higher than for photolithography. The electron beam needs a machine to create a vacuum environment, which is much more expensive. Another disadvantage is that the fabrication efficiency is much lower than for photolithography. Because the electron beam is serial, it can only be used to fabricate micrometer level samples. In fact, there is another nanofabrication method which is cheaper and has higher fabrication efficiency for nanomaterials. It is called colloidal lithography (CL) [26].

CL utilizes lots of nanoparticles as a mask instead of a pattern from an electron beam. The diameter of the nanoparticles can be from 60 nm to 200 nm. After several fabrication steps, each nanoparticle forms one nanostructure unit which is almost the same size as the nanoparticle. Because the nanoparticle mask can be made in a few minutes, it saves lots of time compared with writing by electron beam. Meanwhile, it does not need a special machine to provide vacuum environment. However, CL is limited by the shape of the nanoparticles, which are normally spheres. It is typically used to make simple structures like nanodisks and nanoholes. Recently, the CL got a huge development. With some additional fabrication processes, CL can also be used to produce more complex structures like nanowells and nanopores. In this chapter, all of them will be described.

## 2.1 Fabrication of nanoholes

Short range arrayed nanoholes in a gold film is one of the simplest structures which can be prepared using colloidal lithography. Both the size and periodicity of nanoholes can be adjusted by using different colloidal solutions. Fig.1 shows the basic steps of fabrication of nanohole samples. First step is to adsorb plastic particles on the glass substrate. Because the used plastic particles have negative charges, the negative glass substrate needs positive charges to attract the particles. The positive charges can be supplied by an aluminium chlorohydrate (ACH) solution. The 5% concentration ACH solution should be dropped on the glass substrate first followed by waiting around 1 minute, then rinsing. Next, the colloidal solution is dropped on the substrate and one waits another 2 minutes for the substrate to adsorb particles. To reinforce the stability of the plastic nanoparticles on the substrate, ethylene glycol at 200 °C can be poured on the substrate after absorbing. The second step is metal deposition. 1 nm Cr should be deposited first because it is the adhesion layer between the glass substrate and the gold layer. Cr layer helps gold strongly attach on the glass substrate. Then, a gold layer with thickness of tens of nanometers is deposited. The deposition speed should be around 1 Å/sec. The last layer is Al<sub>2</sub>O<sub>3</sub>, which should be around 15 nm. In step 3, the colloidal particles should be removed by a soft material like a rubber or a sponge. The Al<sub>2</sub>O<sub>3</sub> layer protects the gold surface so that it is not scratched by the soft material. After removing the particles, the last step is to remove the Al<sub>2</sub>O<sub>3</sub> layer. The Al<sub>2</sub>O<sub>3</sub> layer can be dissolved in a 30 mM NaOH solution. The standard way is putting the samples into the NaOH solution and wait around 1 hour. After drying, the nanoholes are ready.

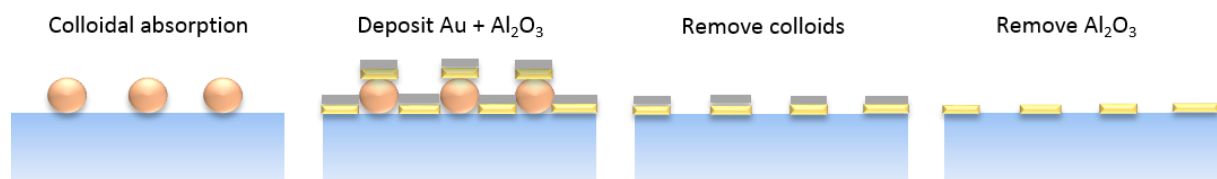


*Figure 1. The process of making simple nanoholes.*

For the nanoholes structure, both the size and periodicity of nanoholes are totally decided by the polystyrene (PS) particles in the colloidal solution. Nanoholes and the monolayer of PS particles have the same size and periodicity. The PS particles with different sizes can be bought directly from companies. The distance between the neighboring particles depends on the amount of charges on the PS particles. In generally, the smaller PS particles have less charges, so the distance between small PS particles is shorter than between large PS particles.

For the size adjustment, different sizes of PS particles can be used to fabricate different nanoholes. However, one disadvantage of this technology is that the size uniformity of PS particles is not good when the particle size is below 100 nm. Fig. 2 shows different sizes of nanoholes which are made by colloidal lithography. It is quite clear that for the 58 nm nanoholes (top left), the size uniformity is quite bad. In fact, lots of nanoholes are larger than 60 nm and the average size of nanoholes is 65 nm. Using very small nanoparticles to get very small nanoholes (<100 nm) seems not to be an effective way. Additionally, the periodicity is very small. However, with increasing the size of PS particles, the uniformity looks much better. The nanoholes with 105 nm (bottom right) have much less size variation than 58 nm nanoholes. In general, the bigger PS nanoparticles always have better size uniformity.

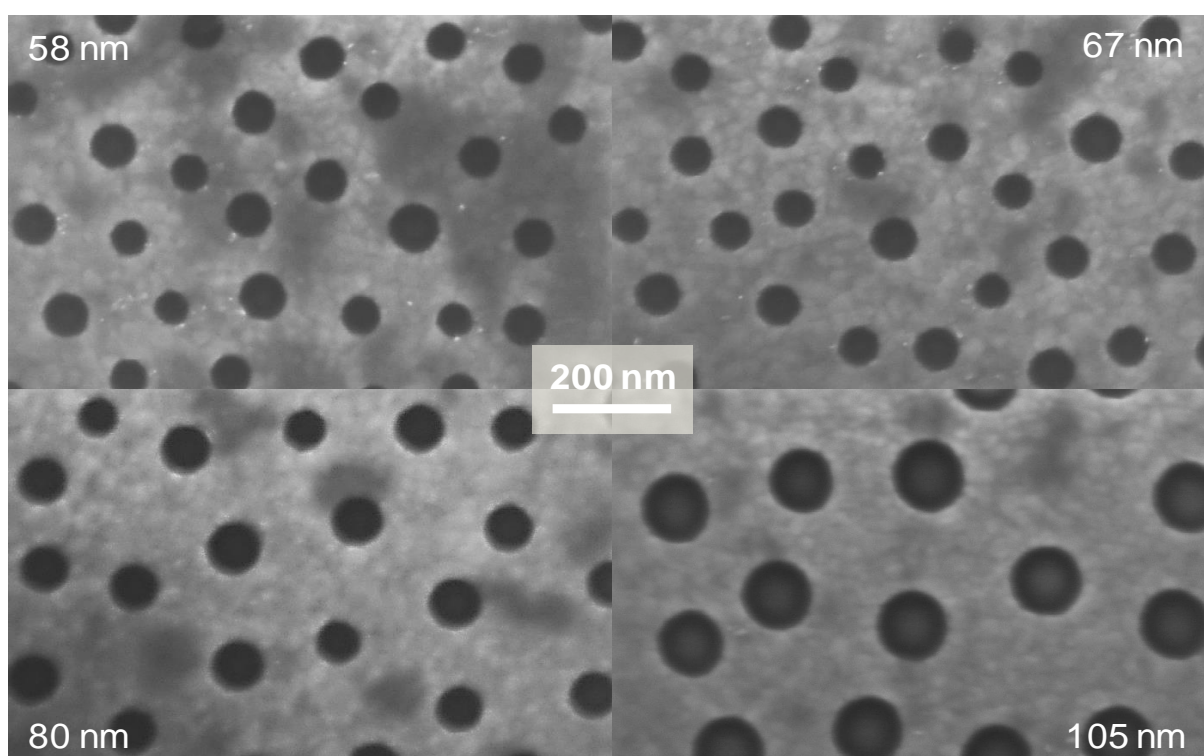


*Figure 2. Different sizes nanoholes were made by different colloidal solutions.*

Recently, one new method which could be used to fabricate uniform small nanoholes was invented [46]. It could conserve the uniformity of large nanoholes and also produce quite small nanoholes which are around 50 nm. The method is based on shrinking the big particles by oxygen plasma after the PS particles are adsorbed on the substrate. After oxygen plasma shrinking, the size of particles becomes much smaller. Because the shrinking rate is quite uniform for the particles and the large particles have relatively uniform size, the shrunk small particles are also quite uniform.

The size of shrunk particles can be adjusted by the shrinking time. The average shrinking speed is around 1 nm/s. Fig. 3 shows the shrinking process. The initial size of PS particles is typically 158 nm. After the particles are absorbed on a substrate, they can become shrunk by oxygen plasma. The plasma power is 50 W, pressure is 250 mTorr, and gas flow is 80 sccm. Since the

initial size of colloidal particles is 158 nm and the average shrinking speed is 1 nm/s, the shrinking time is around 108 s (50 nm particles). One important point when using the oxygen plasma shrinking is that the shrinking speed is not very stable, because the shrinking speed is also related with the surface temperature of nanoparticles and the temperature of the nanoparticles increases during the shrinking process [27]. To get more stable shrinking speed, the best option is cooling the sample after every 10 sec shrinking. Fig. 4 shows how the nanoholes look like. It is obvious that these samples have almost the same uniformity. To compare with the samples directly made by small particles, the diameters of all the holes are measured. Fig. 5 shows the measured diameter histogram. For the samples which are made by particle shrinking, over 90% of the nanoholes are within  $\pm 4$  nm variation, even for 50 nm nanoholes. However, for the nanoholes which are directly made by 58 nm PS particles, the distribution is much wider. In addition, this oxygen plasma shrinking technology could be used for other kinds of nanostructures like nanowells and nanopores.

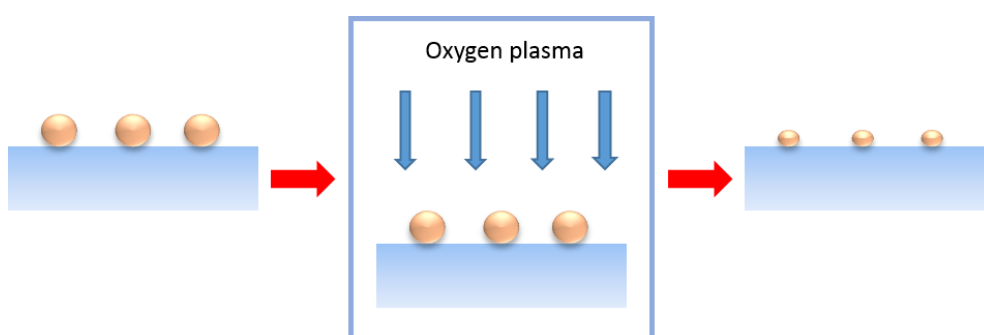


Figure 3. The process of shrinking the nanoparticles to get smaller nanoholes.

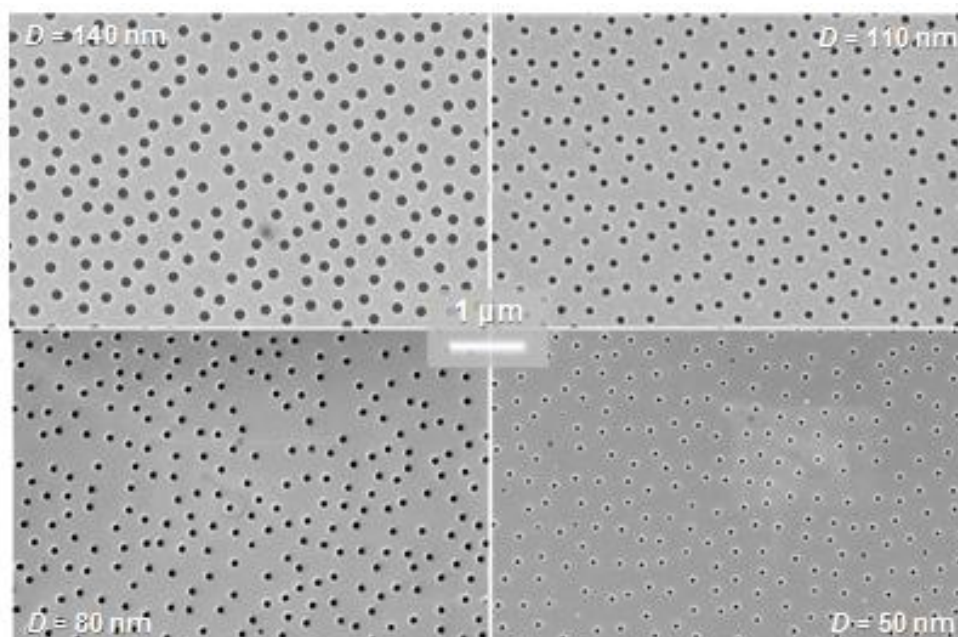


Figure 4. The SEM images include four different nanoholes samples made with the same colloidal solution.

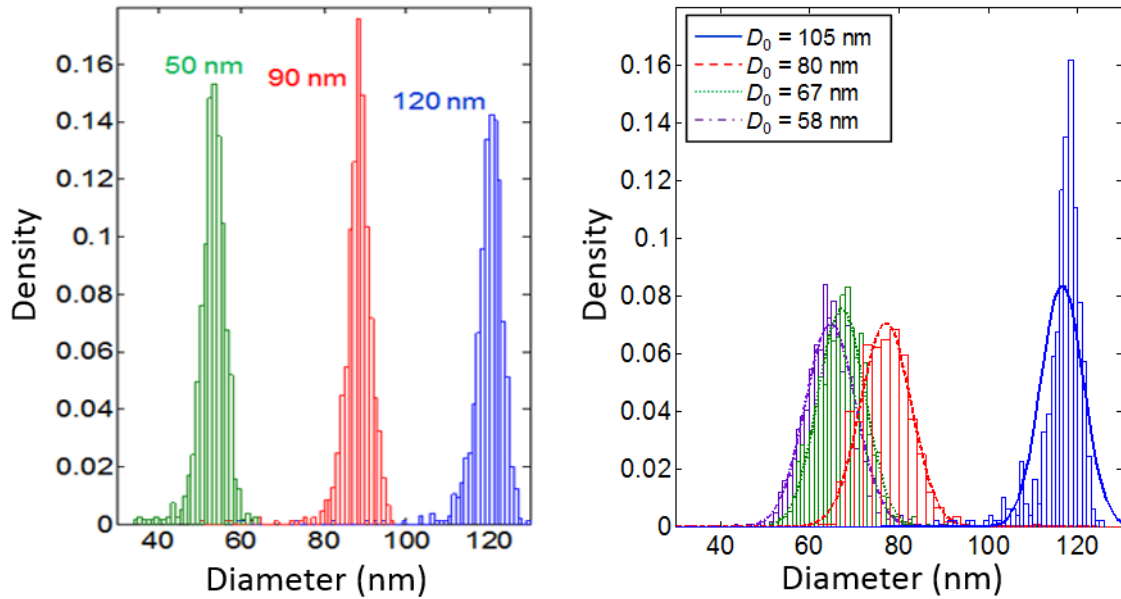


Figure 5. The histograms of measured diameters. The left figure is achieved by using the shrinking technology to get nanoholes. The right figure is achieved by directly using different sizes of PS particles to get nanoholes.

## 2.2 Fabrication of nanowells

The nanowells structure is a further development from the nanoholes. Both of them can be fabricated by colloidal lithography. However, nanowells have one additional  $\text{Nb}_2\text{O}_5$  layer between the gold layer and the glass substrate. Nanowells need a more complex fabrication process, which is shown in Fig. 6. Compared with fabrication of nanoholes, a  $\text{Nb}_2\text{O}_5$  layer should be deposited on the substrate before starting colloidal lithography, which is step 3. This is done by reactive sputtering and a Nb target. The deposition current should be 0.6 A, the process pressure is 7.6 mTorr, the Ar gas flow is 20 sccm and  $\text{O}_2$  flow is 25 sccm. When using this recipe, the deposition speed is around 5 nm/min. In general, the thickness of the  $\text{Nb}_2\text{O}_5$  layer is around 200 nm after 40 minutes deposition. After removing the nanoparticles in step 5, nanoholes are formed. Since the surface of the sample is protected by  $\text{Al}_2\text{O}_3$ , reactive ion etching (RIE) can be used to anisotropically etch the  $\text{Nb}_2\text{O}_5$  layer to form nanowells without destroying the gold layer. The recipe of RIE is 150 W power, 40 sccm  $\text{CF}_4$ , 10 sccm  $\text{O}_2$  and 15 mTorr as

the base pressure. The etching time is 7 minutes. Fig. 7 shows how the nanowells looks like in SEM.

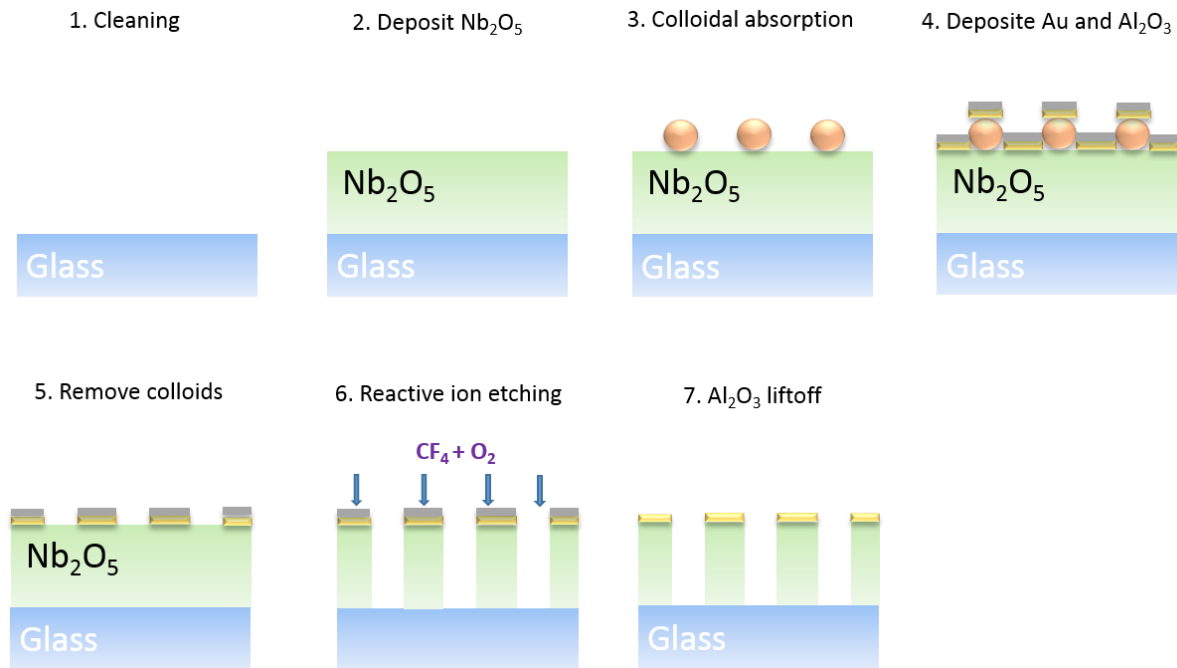


Figure 6. The fabrication process of the nanowells.

In Fig. 7 (B), it is quite clear that the nanowells structure does not have vertical walls. Each nanowell has a cone structure instead of a cylinder. The diameter of the top circle is around 150 nm and the bottom is around 50 nm. Since the thickness of  $\text{Nb}_2\text{O}_5$  is around 200 nm, the depth of the nanowells should also be around 200 nm. It should be noticed that RIE can also etch the gold a little bit. After RIE, the diameter of the gold holes is enlarged from around 107 nm to 150 nm. With higher input power, the enlarging phenomenon would be more obvious. However, the input power also decides the etching depth of nanowells. If the input power is smaller than 150 W, the etching depth of 200 nm is hard to reach in 7 min.

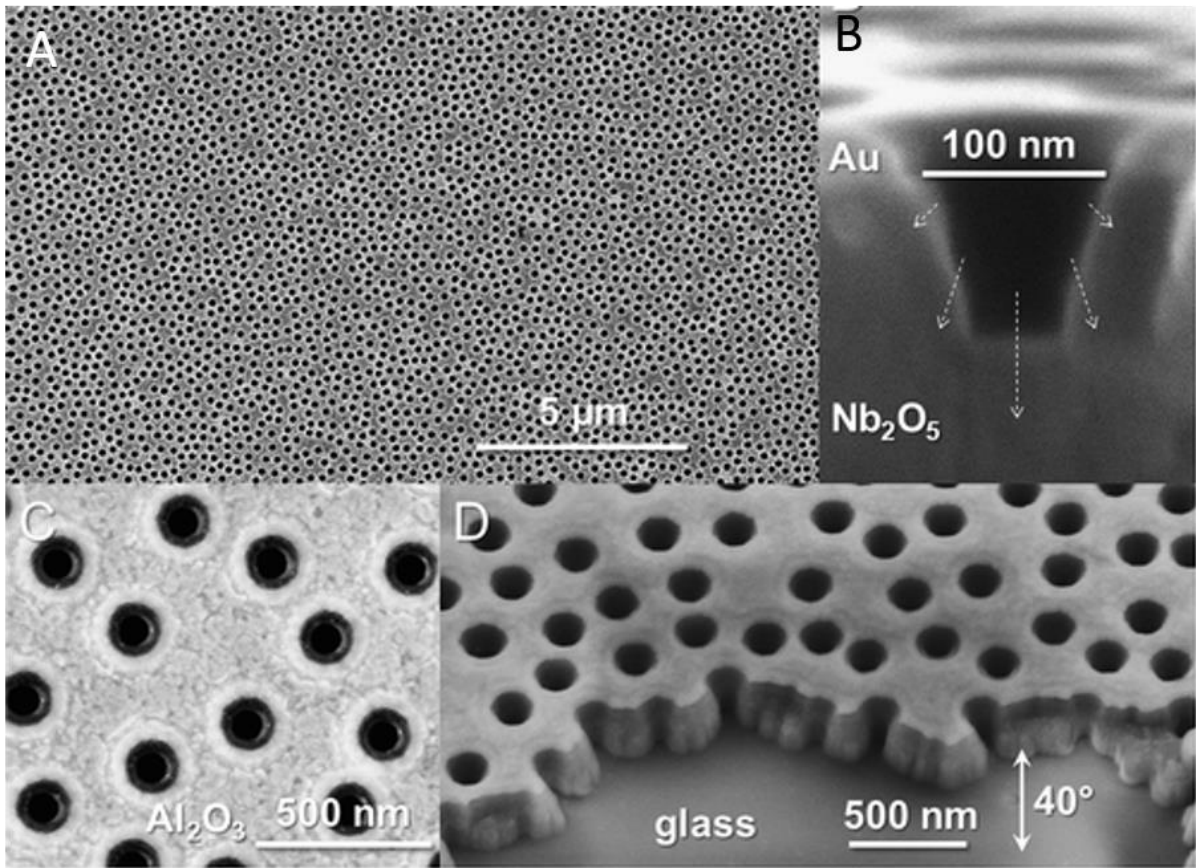


Figure 7. Electron microscopy investigation of fabricated structures: (A) short-range ordered pattern on a large area; (B) cross section of an incompletely etched nanowell; (C) a sample with the  $\text{Al}_2\text{O}_3$  mask remaining, after the dry etch; (D) scratched and tilted sample surface. [Images are from J. Junesch, T. Sannomiya, A.B.Dahlin. ACS Nano 2012 paper]

## 2.3 Fabrication of nanopores

The nanopores are made on a metal-dielectric-metal (MIM) membrane with total thickness of  $\sim 100$  nm. Compared with the nanoholes and nanowells structures, it does not have a glass substrate. The whole structure is suspended on a  $100 \mu\text{m} \times 100 \mu\text{m}$  window supported by a silicon wafer [23]. It also utilizes colloidal lithography to make the basic nanostructure, following by other etching technologies. Nanopores could be used as biosensors and also nanofluidic channels [29].

In comparison with the fabrication process of nanoholes and nanowells, for nanopores it is much more complex. It contains both photolithography and colloidal lithography technology. The standard fabrication process is shown in Fig. 8 excluding the preparation of the window membrane.

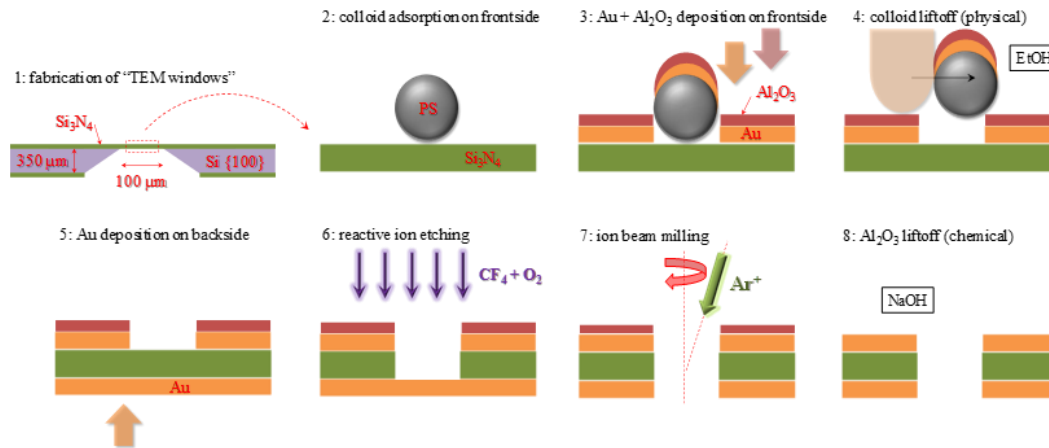
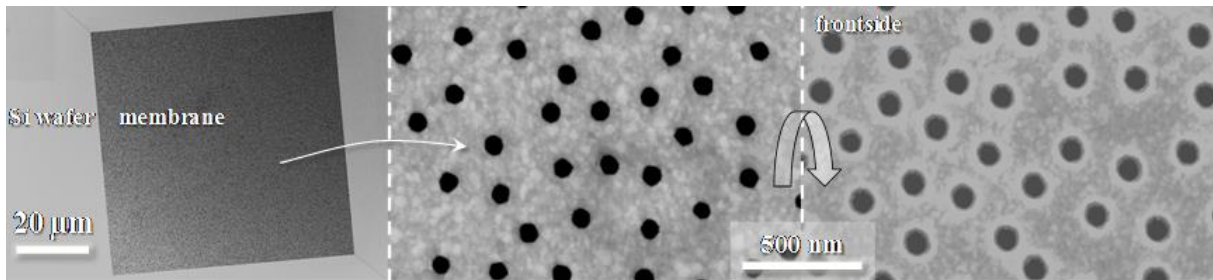


Figure 8. The fabrication process of nanopores.

The fabrication starts with coating a  $\text{Si}_3\text{N}_4$  layer on a Si wafer, which has around  $500\ \mu\text{m}$  thickness. The  $\text{Si}_3\text{N}_4$  layer is made by low pressure chemical vapour deposition (LPCVD) technology. The deposition temperature is  $820\ ^\circ\text{C}$ , pressure is  $250\ \text{mT}$  and flow speed of  $\text{NH}_3$  is  $32\ \text{sccm}$ . The deposition speed is  $5.7\ \text{nm}/\text{min}$ . Since the thickness of  $\text{Si}_3\text{N}_4$  is around  $50\ \text{nm}$ , the deposition time is around  $9\ \text{minutes}$ . It should be noticed that a higher deposition temperature will increase the stability of the  $\text{Si}_3\text{N}_4$  layer. Since when removing PS particles in colloidal lithography it is quite easy to break the  $50\ \text{nm}$   $\text{Si}_3\text{N}_4$  membrane, the  $\text{Si}_3\text{N}_4$  layer should be as stable as possible. However, too high temperature would lead to inhomogeneous thickness of the  $\text{Si}_3\text{N}_4$  layer. For the  $4\ \text{inches}$  wafer, the thickness difference between the center and boundary area is around  $7\ \text{nm}$  under  $820\ ^\circ\text{C}$  deposition temperature. After deposition of the  $\text{Si}_3\text{N}_4$  layer, photolithography is used to write square patterns with  $0.804\ \text{mm}$  as side length on the backside of the wafer. Then, the wafer is put in  $35\%$  KOH solution at  $80\ ^\circ\text{C}$ . In general, after  $10\ \text{hours}$  etching, the  $\text{Si}_3\text{N}_4$  membrane should form. Since the KOH etching forms a wall with a defined angle relative to the crystal plane of the Si, the final membrane size is around  $100\ \mu\text{m}$ . Step 4 is the most difficult part of this fabrication. Since the membrane is just a few tens of nanometers in thickness, it is quite easy to break the membrane by using the normal way to remove particles. Specially, photoresist (S1813) can be used to coat on the back side ( $0.804\ \text{mm}$  side) of the membrane. The photoresist can enhance the stability of the  $\text{Si}_3\text{N}_4$  layer to avoid breaking it during step 4. It should be noticed that the photoresist should be removed before step 7, otherwise, ion beam milling (IBM) cannot totally remove the bottom side gold to form the pore because of the photoresist protection. In step 6, the middle  $\text{Si}_3\text{N}_4$  layer is etched away by RIE. The recipe is quite different compared with etching the  $\text{Nb}_2\text{O}_5$  layer of nanowells. The gas speed of  $\text{CF}_4$  is  $30\ \text{sccm}$  and  $\text{O}_2$  is  $20\ \text{sccm}$ . The etching time should be  $9\ \text{minutes}$  and the etching power is  $50\ \text{W}$ . Fig. 9 shows how the nanopores look like by SEM. Similar to nanowells,

the nanopores do not have vertical walls. The diameter of the front side holes is around 120 nm and 80 nm for the back side holes.



*Figure 9. The SEM figures of the nanopores. The holes are observed from both of the front and back sides. [Images are from A. B. Dahlin, M. Mapar, K. Xiong, F. Mazzotta, F. Höök, and T. Sannomiya, Adv. Opt. Mater 2014 paper]*



# Chapter 3

## 3. Plasmonic properties

In chapter 2, the fabrication technologies of nanoholes, nanowells and nanopores are presented. One big reason for fabricating nanomaterials is that they can provide plasmonic signals, which can be used as sensors [29, 30]. The plasmonic signals come from electronic oscillations which are excited by photons. Since different photons can excite different oscillation modes, photons with different frequencies can give different extinction when passing through the material. The spectrum of nanoholes, nanowells or nanopores will have two special points, one is the peak wavelength which represents the frequency of photons with maximum extinction and one dip wavelength which shows the minimum extinction frequency of photons. Both the peak and dip positions are sensitive to the surface conditions of the nanomaterial, which always has red shift after different targets have bound to the surface [31, 32, 33]. Depending on the shifting, the nanomaterials can be used as sensors to detect targets.

### 3.1 Plasmonic signal of nanoholes

The electronic oscillation is influenced by the geometry of the nanostructure [33]. Since mainly the incident photons with the right wavelength interact with the nanostructure, the electrons of the nanomaterials are sometimes in resonance with incident photons, which induces strong plasmonic modes. For different nanostructures, the plasmonic signals can originate from different modes. Since this thesis focuses on the nanoholes, nanowells and nanopores structures, this chapter will just introduce the plasmonic modes of these nanostructures.

Fig. 10 shows how the plasmonic modes are excited in the nanoholes structure by incident photons. When the photons reach at the nanoholes surface, they can transform their momentum and energy into the electron oscillations of the metal. Some energy will be absorbed inside of the metal because of the collisions of the electrons inside. The other energy and momentum can be transported along the interface of the metal and dielectric, which would form the surface plasmonic polaritons (SPPs) [34]. For the nanoholes structure, the SPPs can travel from one hole to the neighboring hole along the interface, then the SPPs can interfere with the incident light on the neighboring holes and change the intensity of the transmitted light.

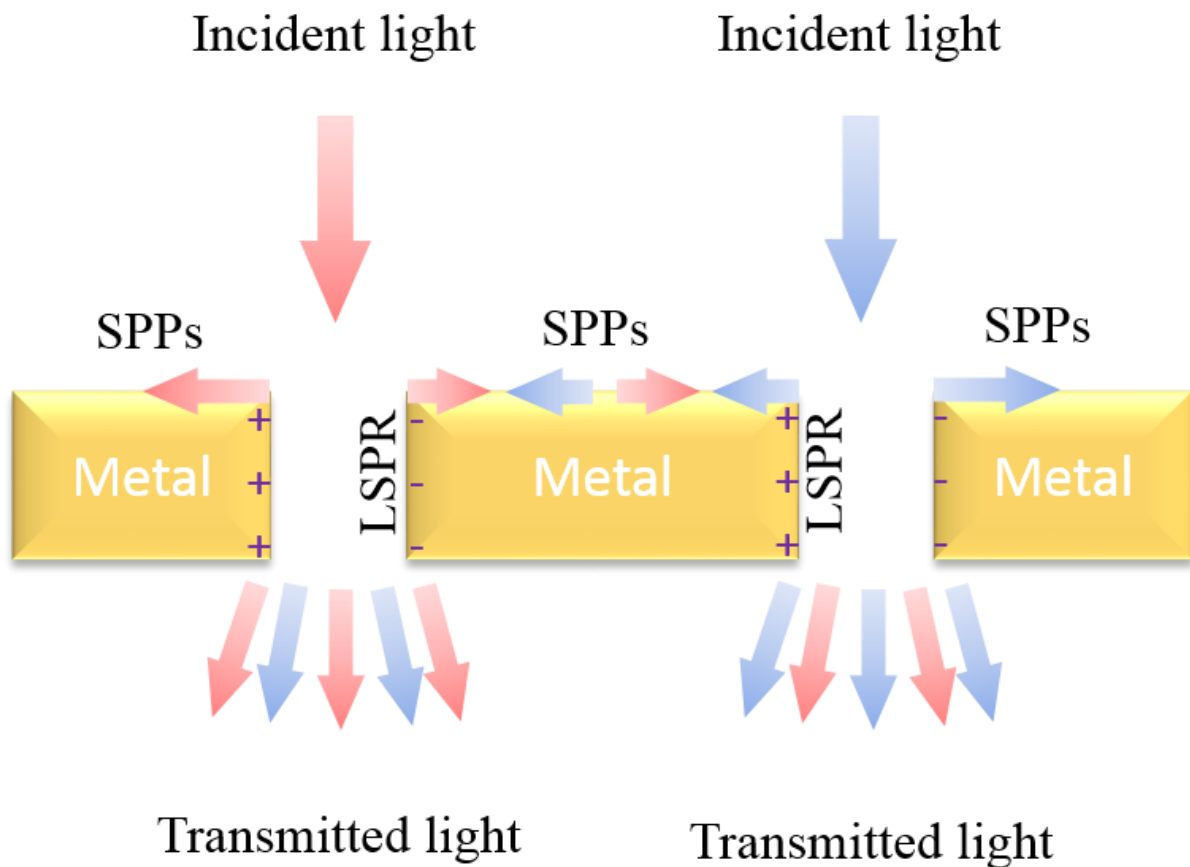


Figure 10. The plasmonic mode of the nanoholes structure.

To excite the plasmons, the material should include both a metal and a dielectric. It should be noticed that the plasmons can not be excited on a metal surface without a nanostructure, because the momentum of incident photons is smaller than for the plasmons [35]. At a planar surface dividing two semi-infinite materials, the wave vector,  $k_{SPP}$ , of the SPPs with wavelength  $\lambda$  depends on the dielectric function of the metal [36],  $\epsilon_m$ , at that wavelength and the refractive index of the surrounding medium,  $n$ , according to the dispersion relation:

$$k_{\text{SPP}} = \frac{2\pi}{\lambda} \sqrt{\frac{\epsilon_m n^2}{\epsilon_m + n^2}} \quad (1)$$

The incident photon travels in a medium with the same refractive index  $n$ . The component of the wave vector which is parallel to the planar metal/dielectric interface is:

$$k_{\text{photon}} = \frac{2\pi}{\lambda} n \sin(\theta) \quad (2)$$

where  $\theta$  is the angle of incidence. If the photon has normal incidence,  $k_{\text{photon}}$  would be 0. Even if the incidence angle is 90 degrees, so that  $k_{\text{photon}}$  will be  $2\pi n/\lambda$ ,  $k_{\text{SPP}}$  is still larger than  $k_{\text{photon}}$  since  $\epsilon_m$  is negative and larger in magnitude than  $n$  ( $n \geq 1$ ).

One of the most common ways to excite plasmons by normal incidence light is to fabricate periodic nanostructures which are smaller than the incident wavelength on the metal surface. The nanostructure can lead the refraction of the incident light, which can increase the component parallel to the metal surface of the photon momentum to excite the plasmons. For the nanoholes structure, the plasmons are excited at the nanoholes and form SPPs, which spread along the metal/dielectric interface. The new wave vector at normal incidence would then be:

$$k_{\text{photon}} = \frac{i2\pi}{\Lambda} \quad (3)$$

where  $\Lambda$  is the lattice constant and  $i$  is a nonzero integer number representing the scattering orders from the grating-like structure. Since the grating increase the momentum ( $\Lambda \leq \lambda$ ) of the photons, the SPPs can be excited in the nanoholes nanomaterial.

The SPPs can influence the extinction spectrum (transmitted light) of the nanoholes structures. Since SPPs can travel along the metal/dielectric interface and reach to the neighboring holes, there is interference with the incident photons on the neighboring nanoholes, which changes the extinction spectrum. Because of the half wave loss, if the phase of the SPPs is then equal to  $2\pi i$  ( $i$  is integer number) of the incident photons phase, the transmitted light would be weakest, where is the peak position of the extinction spectrum. Thus, the wavelength of the peak position can be estimated by the function

$$\Lambda = \frac{2\pi i}{\text{Re}(k_{\text{SPP}})} \quad (4)$$

where  $A$  is the average distance to the neighboring holes (effective periodicity for short-range order). If one only considers the condition  $i=1$ , then equation (4) would be  $A = \lambda_{SPP}$ . Fig. 11 shows the relationship between  $\lambda_{SPP}$  and  $\lambda_{photon}$ , which is calculated based on the structure of a 30 nm gold film on a glass substrate in air. Since the refractive index of gold is wavelength dependent, the relationship is not linear. In general in this work, the nanomaterial of nanoholes with 158 nm diameter and 320 nm periodicity is used as the plasmonic sensor. Based on the dispersion relation, when  $A=320$  nm, the peak position should be around 640 nm. Fig. 12 shows the extinction spectrum of such a nanoholes sample.

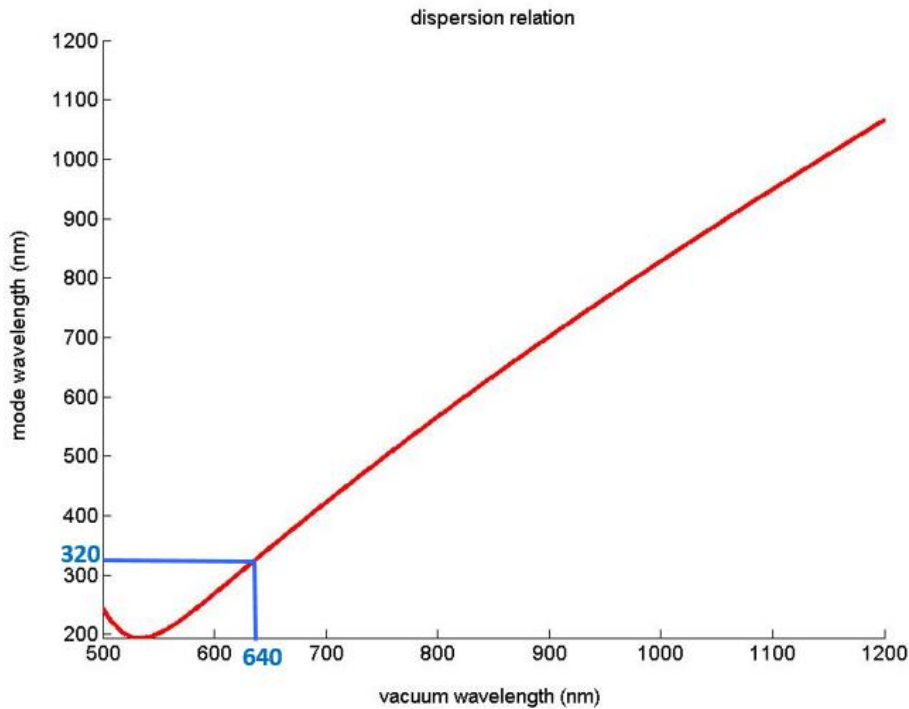


Figure 11. The relationship between the mode wavelength ( $\lambda_{SPP}$ ) and vacuum wavelength ( $\lambda_{photon}$ ).

In the Fig. 12, it is quite clear that the peak position is around 650 nm, which is a little red shifted compared with the expected value. This is likely because the dispersion relation is influenced by the presence of holes in the gold film [51]. Based on the results in the last paper, it is quite clear that the peak position of the extinction spectrum is mainly related with the periodicity of nanoholes. However, the dip position is mainly influenced by the diameter of nanoholes. This has been verified with nanoholes samples with the same periodicity and different diameters, fabricated using oxygen plasma shrinking technology. Fig. 13 shows the extinction spectrum of such nanoholes samples.

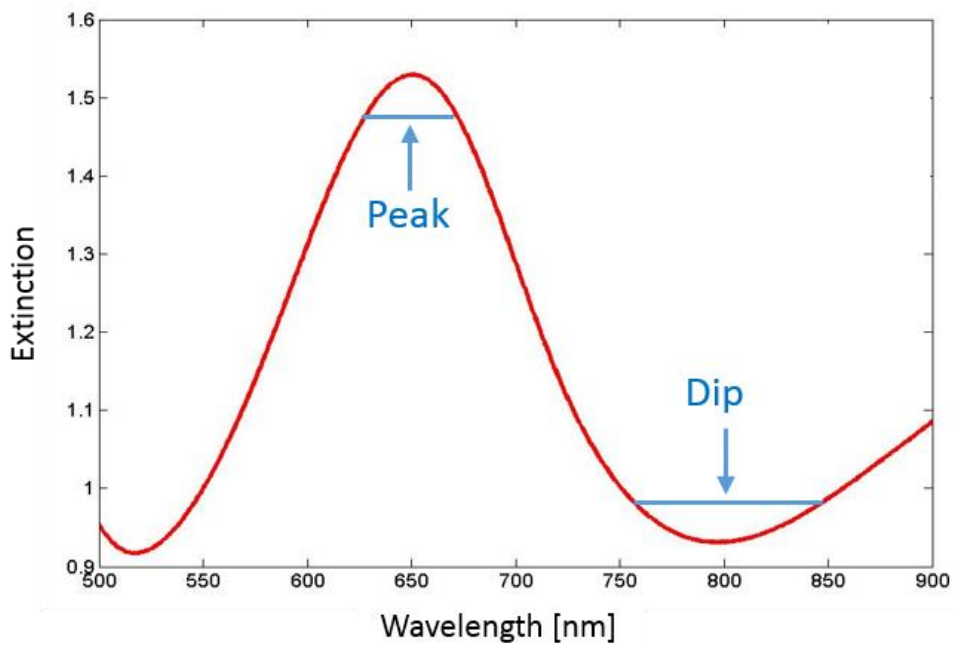


Figure 12. Plasmonic signal of nanoholes with 150 nm diameter, 320 nm periodicity and 30 nm thickness.

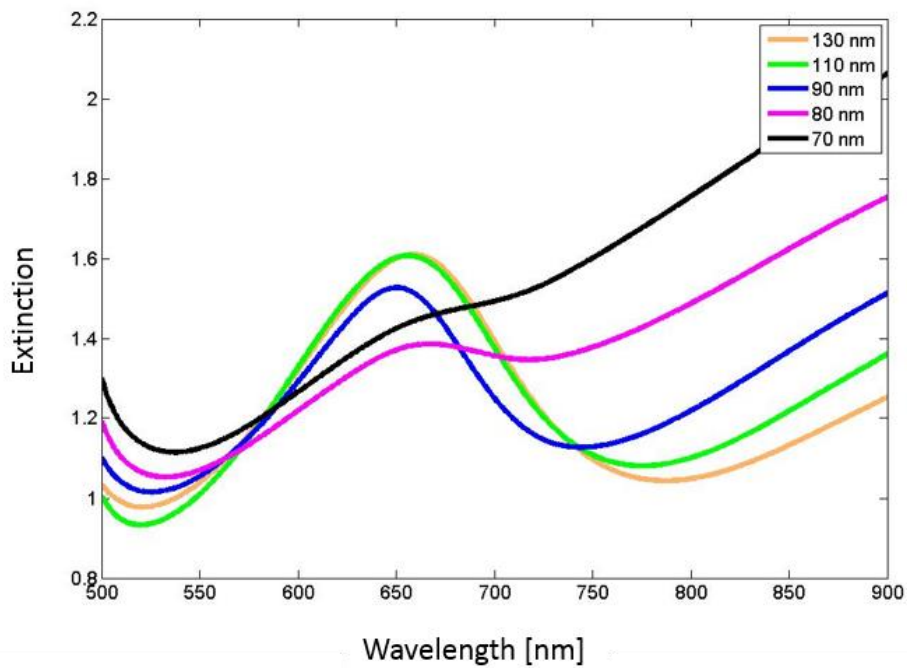


Figure 13. The spectrum of different nanoholes samples. The diameter changes from 130 nm to 70 nm. The periodicity is constant 320 nm and the gold thickness is 30 nm.

It is quite clear that the peak positions of nanoholes with different diameters are almost the same, around 650 nm. However, the dip positions have obvious blue shifting with decrease of the diameter. In fact, the dip position is more related with localized surface plasmon resonance (LSPR) [37], which can transform the incident light wave into a scattered light wave. Since the scattering light is the main part of the transmitted light, the photon with strongest LSPR would be the dip position.

For a metal nanoparticle, the wavelength of the photon with strongest LSPR can be calculated by the function [47]:

$$\text{Re}\{\varepsilon_m + L[\varepsilon(\lambda_{\text{LSPR}}) - \varepsilon_m]\} = 0 \quad (5)$$

where  $\varepsilon_m$  is the relative permittivity of the environment and  $L$  is a geometrical constant ( $0 < L < 1$ ). For the nanoholes, one can assume that  $L \propto h/D$ , in analogy to nanoparticles, where  $D$  is the diameter of the nanoholes. Then,  $\varepsilon(\lambda_{\text{LSPR}}) \propto D/h$  and  $\lambda_{\text{LSPR}} \propto D/h$  for small changes, so the dip position should have a redshift with increasing diameter of the nanoholes.

Except for the geometrical structure influence on the peak and the dip positions of the spectrum, the refractive index of environment can also affect them. For the environment with higher refractive index, both of the peak and the dip will have red shifts. Fig. 14 shows the relationship between the shifts and the refractive index of the environment. Nanoholes samples with two different diameters, 60 nm and 160 nm are used. In this experiment, different water solutions with an increasing amount of glycerol (5, 10, 15, 20, 25, 30 and 35 percent by weight) are used to change the refractive index of the environment. With higher concentration, the refractive index will increase and cause constant red shifts on the peak and the dip positions. In Fig. 14 (B), it is quite clear that the amount of shifts for the peak and the dip is not very related with the diameter of the nanoholes.

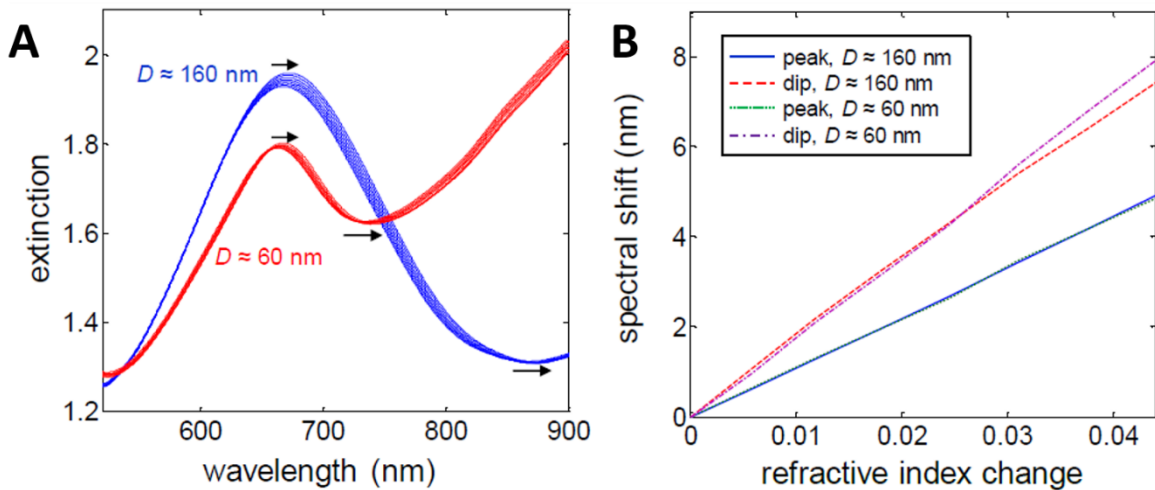


Figure 14. The relationship between the shifts and the refractive index of the environment.

### 3.2 Plasmonic signal of nanowells

The plasmonic signal of the nanowells is quite similar to nanoholes. It also has one peak and one dip in the extinction spectrum. Fig. 15 shows the spectrum of the nanowells and the dispersion relation between  $\lambda_{SPP}$  and  $\lambda_{photon}$ . The diameter of the nanowells is approximately 100 nm, the periodicity is 230 nm, the thickness of gold is 30 nm and Nb<sub>2</sub>O<sub>5</sub> is 200 nm. Based on the dispersion relation, the expected peak position is almost the same as in experimental data, which is around 710 nm. The nanowells structure has a very special electromagnetic field distribution. Different regions of nanowells have different sensitivities for peak and dip shifts [45]. Fig. 16 shows the different sensitive regions and the peak and dip shifts of a dielectric binding on these regions. The thickness of the dielectric is 5 nm and its refractive index is 1.5.

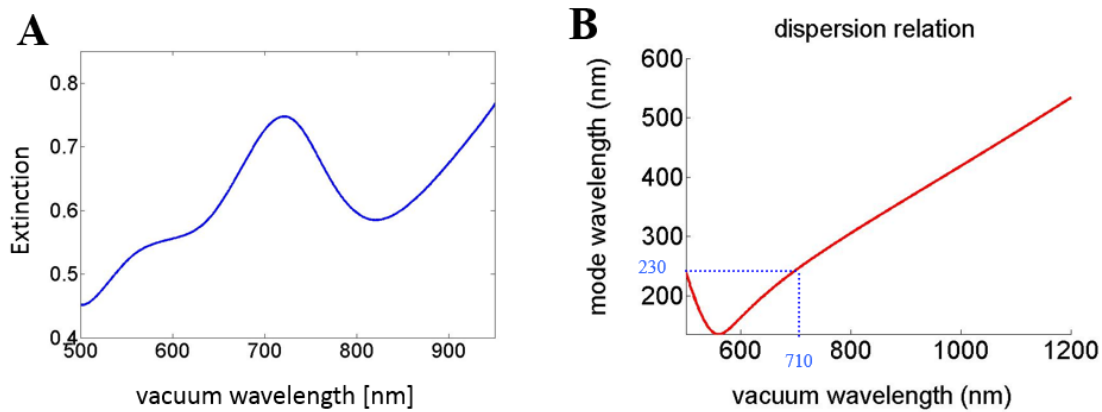


Figure 15. (A) The spectrum of the nanowells. (B) The dispersion relation of  $\lambda_{SPP}$  and  $\lambda_{photon}$ .

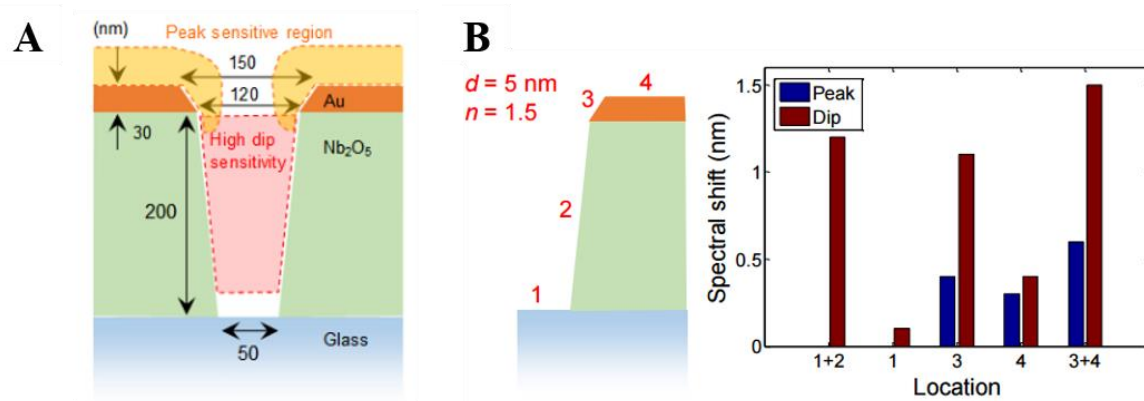


Figure 16. (A) The sensitive regions of plasmonic signals. (B) The peak and dip shift of binding dielectric on different regions.

In Fig. 15 (B), it is quite clear that the sensitive region of the dip is much larger than that of the peak. In the wall of the Nb<sub>2</sub>O<sub>5</sub> layer (region 2), there is no peak shift after introducing the dielectric. Based on the simulations, the dip shift is around 1.3 nm after the dielectric covering the whole region 1 and 2. The region on the gold layer (regions 3 and 4) have both peak and dip shifts after binding. The simulations show 0.7 nm peak shift and 1.5 nm dip shift if the dielectric covers all the region 3 and 4. In principle, the ratio between the dip and peak shifts can be used to determine if binding occurs preferentially inside the nanowells.

### 3.3 Plasmonic signal of nanopores

The nanopores in this work have a more complex optical signal in comparison with the nanoholes structure, since it has two gold layers close to each other. The extinction spectrum is influenced by both layers [22]. Fig. 16 shows two different transport modes, which show different charge distribution conditions of top and bottom layers. The low energy hybridized bonding mode (LEHB) shows the antisymmetric charge distribution of the top and bottom gold layers and the high energy hybridized bonding (HEHB) mode shows the symmetric charge distribution. However, exciting the LEHB mode is hard since the distance between two gold layers is just 50 nm, which cannot create enough phase delay to match the antisymmetric charge distribution. However, the hybridized bonding mode (HEHB) is much easier to excite, since the small phase delay should lead to an almost symmetric charge distribution. Comparing the plasmonic signal with the nanoholes and nanowells, the nanopores have a weaker signal since it has the additional condition that the phase difference between top and bottom SPPs should be small enough. Another reason is that the damping of the SPP mode can be stronger than nanoholes and nanowells. Fig. 17 shows the plasmonic signals of nanopores samples with different geometries.

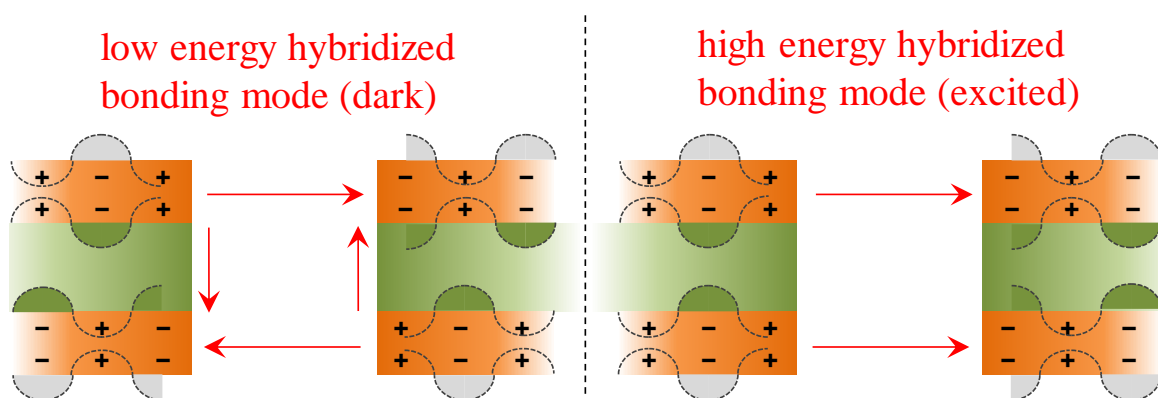


Figure 16. Qualitative description of the charge distributions for the surface plasmon modes. [Images are A. B. Dahlin, M. Mapar, K. Xiong, F. Mazzotta, F. Höök, and T. Sannomiya, *Adv. Opt. Mater* 2014 paper]

In Fig. 17, the arrows indicate the resonance wavelengths for the bonding surface plasmon modes.

As predicted by the theory of arbitrary multilayer dispersion relations [37], the arrows pointing up show the predicted peak position of the HEHB mode. Ordinary arrows pointing down show the predicted peak of the LEHB mode. The dotted arrows correspond to the bonding mode of the same single gold film on a membrane which is semi-infinite. Since the LEHB is weak, the peak of LEHB cannot be detected experimentally but it can be seen in simulation. When comparing with one gold layer structures, the peak of the two gold layers structure has a blue shift. For the different nanopores samples, it is quite clear that the peak has a red shift with increasing the periodicity, which is similar to nanowells and nanoholes.

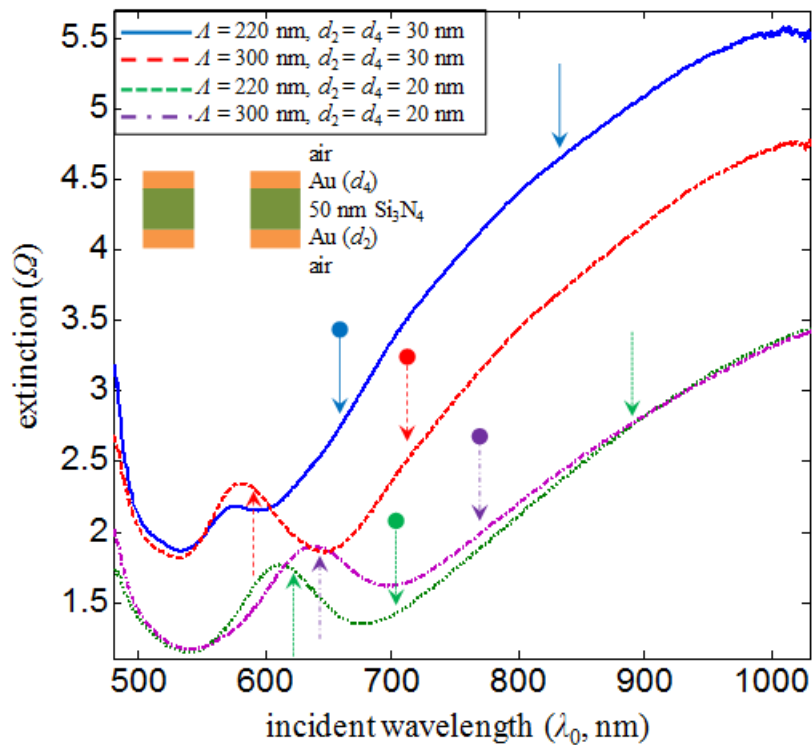


Fig. 17 shows the plasmonic signal of nanopores samples with different geometries. [Images are A. B. Dahlin, M. Mapar, K. Xiong, F. Mazzotta, F. Höök, and T. Sannomiya, *Adv. Opt. Mater* 2014 paper]



# Chapter 4

## Implementing electronic techniques

Plasmonic samples are always formed by both a dielectric and a metal, since the plasmonic modes can only be excited on the interface between the dielectric and metal. Besides providing plasmonic signals, the nanomaterials with continuous metal film could also have lots of other applications after combining them with electronic technologies. In this chapter, the thermal plasmonic sensor platform will be introduced [23]. It utilizes the resistance of the metal film so that lateral applied electrical voltages produce thermal energy to form a thermal source (hot plate). This technology could be used for fundamental research in thermoplasmonics and also as a thermal source to heat targets.

Fig. 18 shows how to build the thermal plasmonic sensor. In this system, a sample with the nanoholes structure is used. The voltage is applied from the short edges. The temperature can be measured by a thermal camera or calculated by the change in resistance from the IV curve. Plasmonic signals are measured by a spectrometer. The diameter of the nanoholes is around 100 nm and the metal thickness is 30 nm. Silver conductive paste is used to cover the short edges for a homogeneous current distribution. After applying a voltage on the sample, the electrical current will be formed and kept to create thermal energy, which is related to the resistance of the sample. The resistance of the nanoholes could be adjusted by the density of the holes [48]. A higher density of holes will increase the resistance. The thermal energy can be directly calculated by the function  $W=V \times I=V^2/R$ , where  $W$  is the thermal power,  $V$  is the applied voltage,  $I$  is the electrical current and  $R$  is the resistance. It is quite clear that for a given voltage the thermal energy (and the temperature) will decrease with increasing resistance. Similarly, the resistance will decrease when increasing the metal thickness and the temperature would then also increase.

For fundamental research, figuring out the accurate relation of the plasmonic signal shift and metal temperature is a big challenge. It is hard to find an efficient way to heat nanomaterials. Some researchers use light power to heat nanoparticles, since nanoparticles have quite strong absorption for photons with the resonant wavelength, which can produce the thermal energy [38]. However, this requires focusing the light beam into a diffraction limited spot and only single wavelength light sources can be used, which do not provide the spectrum of the nanoparticle. So it is very hard to analyze the relation between the temperature and the plasmonic signal by using this method. Another option is to heat the particles in an oven [39]. Then the whole system would be put in, which makes it quite hard to get accurate results since

the other equipment is also heated. The thermal plasmonic sensor presented here could solve these problems properly.

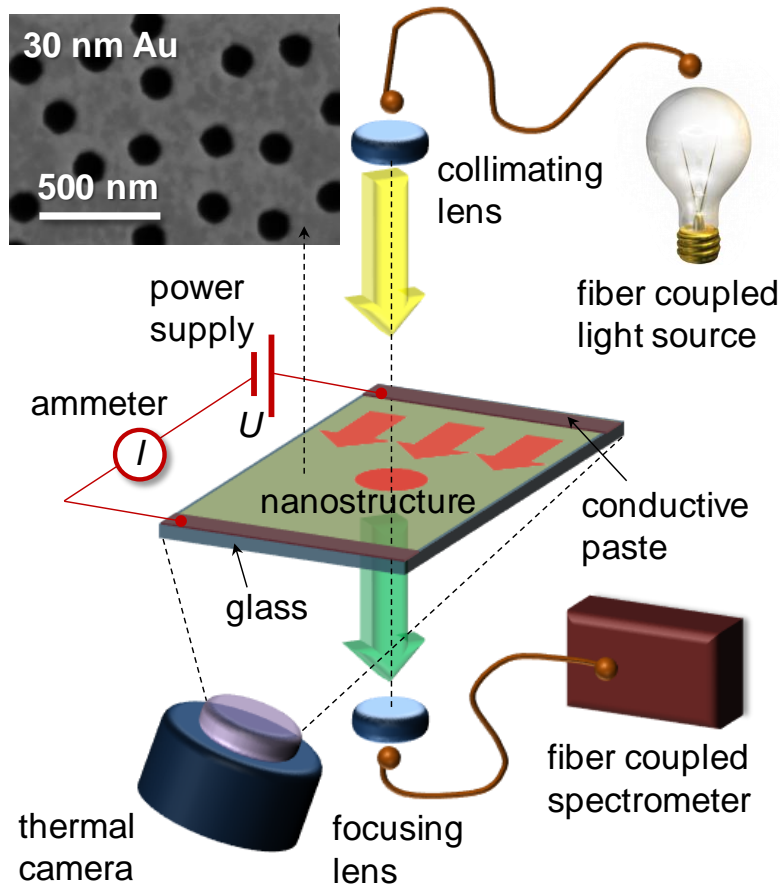


Figure 18. The setup of the thermal plasmonic sensor. [Images are from M. Virk & K. Xiong, M. Svedendahl, M. Käll, and A.B. Dahlin, *Nano Letters* 2014 paper]

Fig. 19 shows both the plasmonic signal variation due to an electrical current and the relation between the peak shift and temperature increase. In Fig. 19 (A), the peak position of the plasmonic sample starts to shift after applying the electrical voltage. The peak needs some time to reach a stable state due to the heat capacity of the supporting glass. When increasing the current, the stable temperature of the metal is higher. It can even reach to around 200°C for a 0.869 A current. In Fig. 19 (B), the relation between the peak shift and temperature is shown, which is quite linear. To investigate the reason for this, one needs to first calculate the relation between the permittivity of gold and temperature. Because the structure of the nanomaterial is not changed, the only reason of peak shift should come from the variation of the metal

permittivity (the variation of refractive index of the environment can be neglected). The permittivity of the metal can be calculated by a Drude model [40]:

$$\varepsilon(\omega) = \varepsilon_{\infty} + \sum_i \varepsilon_{\text{band } i}(\omega) - \frac{\omega_p^2}{\omega[\omega + \gamma i]} \quad (6)$$

Here  $\omega_p$  is the plasma frequency and  $\gamma$  is the damping term for the free electron movement.  $\varepsilon_{\infty}$  is a dielectric constant (usually  $1 \leq \varepsilon_{\infty} \leq 10$ ).  $\varepsilon_{\text{band}}(\omega)$  is also assumed to be independent of  $T$ . Only  $\omega_p$  and  $\gamma$  are related with  $T$ . However,  $\gamma$  would mainly influence the imaginary part of the permittivity, it would broaden the width of the peak rather than causing a peak shift.  $\omega_p$  is more related with the real part of the permittivity, which will influence the peak position. It can be calculated by the function [49]:

$$\omega_p(T) = \frac{\omega_p(T_0)}{\sqrt{1 + 3\beta[T - T_0]}} \quad (7)$$

Here  $\beta$  is the thermal expansion coefficient, which represents the volume expansion with increasing temperature. In Fig. 19 (B), it is quite clear that when the thermal expansion coefficient value of the nanomaterial metal is 2.5 times of the bulk metal, the theoretical peak shift is almost the same as in the experiment. This shows that the thermal expansion value can change when the thickness reaches to nanolevel and it could be measured by the peak shift of the plasmonic signal.

Another application of this thermal plasmonic sensor is heating targets like when on a hotplate. Fig. 20 shows utilization of the system to desorb alkanethiol self-assembled monolayers (SAMs) [41]. The thiol group of SAMs can be assumed to be the link between the gold surface and the alkane chain. The alkanethiols can be transformed into the gas phase by heating. So when the thermal plasmonic sensor system starts to produce thermal energy, the alkanethiol will be gasified which leads to the desorption of the SAM from the metal surface. In Fig. 20, it is quite clear that the peak has a big blue shift during the heating. This is because the process of desorbing SAMs will decrease the refractive index on the metal surface, which makes the plasmonic peak blue shift. The red and blue shifts when turning on and off the applied voltage are just like in Fig. 19 (A).

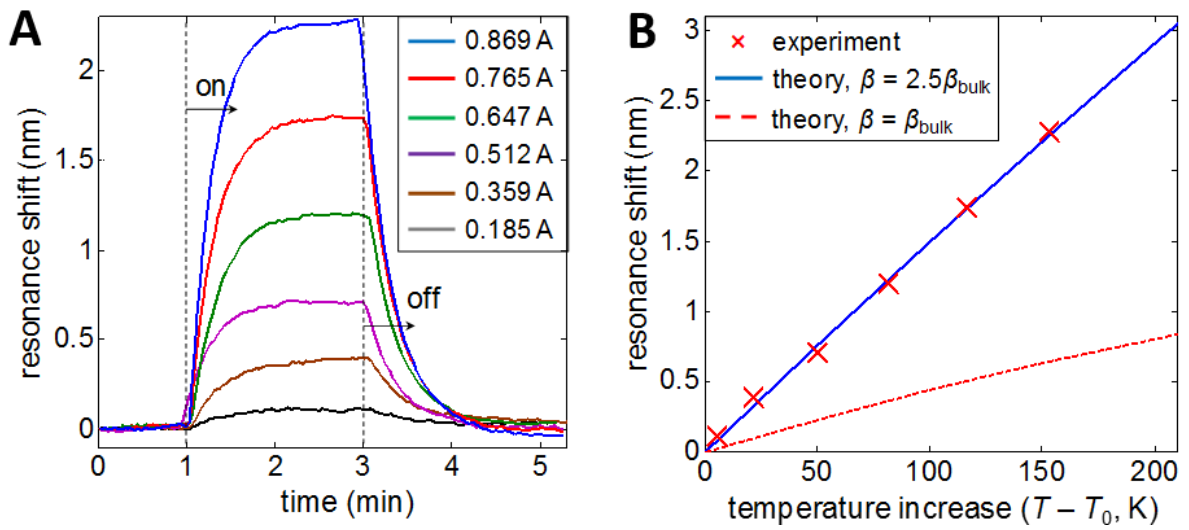


Figure 19. (A) The shift of plasmonic resonance (peak) after applying different voltages. (B) The relation between the plasmonic resonance (peak) shift and temperature. [Images are from M. Virk & K. Xiong, M. Svedendahl, M. Käll, and A.B. Dahlin, Nano Letters 2014 paper]

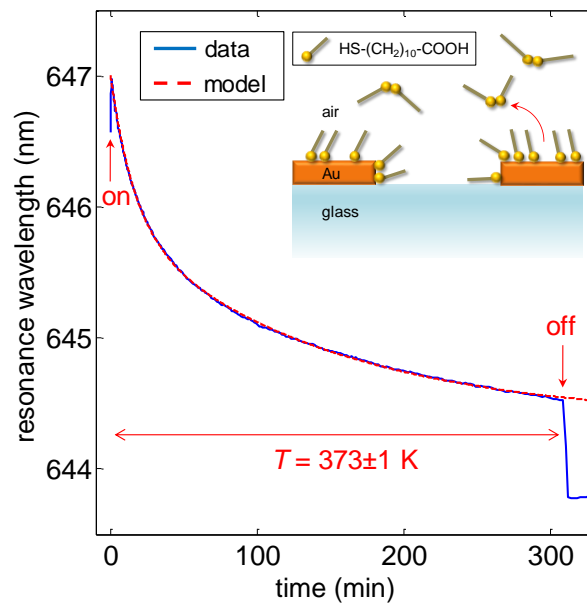


Figure 19. The variation of plasmonic signal while turning on applied voltage. [Images are from M. Virk & K. Xiong, M. Svedendahl, M. Käll, and A.B. Dahlin, Nano Letters 2014 paper]

# Chapter 5

## Summary and Outlook

In this thesis, we introduce new plasmonic biosensors, which includes fabrication technologies, signal analysis and applications. For the fabrication part, three nanomaterials are described which are the nanoholes, nanowells and nanopores. All of them are fabricated based on the colloidal lithography technology, which utilizes plastic particles as a mask to create short-range ordered nanoholes in the metal layers. In comparison with electron beam lithography, it is much faster and cheaper. For different nanostructures, different additional fabrication technologies should be used such as reactive ion etching and ion beam milling. After introducing the fabrication part, the plasmonic signals of these three nanostructures are analysed. The nanostructures provide enough momentum to excite plasmonic modes which can travel along the interface between the metal and dielectric layers, so called surface plasmon polaritons. Another resonance is called localized surface plasmon resonance (LSPR), which can transform the incident light wave into a scattered light wave. Because of the plasmonic modes, the extinction spectrum of the nanostructures has two important features, which are the peak wavelength (maximum extinction) and the dip wavelength (minimum extinction). They are quite sensitive to the surface condition of the sensor and red shift if targets bind on the sensor. For different nanostructure geometries, the peak and dip have different amplitudes and positions because of the different plasmonic modes. Meanwhile, different nanostructures may also have different functions, like nanofluidics through nanopores. Additionally, the plasmonic technology can be combined with other technologies to create lots of new applications. The electronic technology is one good option for structures with continuous metal films. By combining the nanohole samples with electronic heating technology, a thermal plasmonic sensor is built up. The temperature of the sample will increase as a voltage is applied because of the resistance of the thin metal film. The sensor can provide both plasmonic signals and measurements of the surface temperature, which can be used to investigate the thermal material properties of the thin metal film. Another application of this kind of thermal plasmonic sensor is heating targets like a hot plate. SAMs are desorbed from the metal surface by heating the sensor and this process can also be observed by the sensor though detecting the variation of the plasmonic signal.

In the future, more technologies will be involved in the plasmonic biosensor technology. The polymer technology would be one of them. Polymers as organic materials can be designed with a nanometer level thickness. It can bind on the gold surface by using the thiols as reactive groups. Polyethylene glycol (PEG) [42] is one such polymer. If the PEG can bind on the nanopores

structure which is used as a nanofluidic channel, it can form a passive gate to control if molecules pass or if the channel is blocked. In addition, by choosing different kinds of polymers like poly(*n*-isopropylacrylamide) (PNIPAM) [43] and polypyrrole [44], an active gate could be created. PNIPAM is a thermo-responsive polymer and polypyrrole is a conductive polymer. They can change their thickness in different temperatures or at different applied voltages by ion doping. After binding PNIPAM and polypyrrole on nanopores, the size of the resulting nanofluidic channels could be adjusted by applying voltages on the gold layers because it would change both the temperature and doping state of the polymers.

## References

1. A. B. Dahlin, Plasmonic Biosensors: An Integrated View of Refractometric Detection. *Washington* (2012).
2. H. Bayley and P.S. Cremer, Stochastic sensors inspired by biology. *Nature* 413 (2001), 226-230.
3. L. C. Clark, R. Wolf, D. Granger, and Z. Taylor, Continuous recording of blood oxygen tensions by polarography. *Journal of Applied Physiology* 6 (1953), 189-193.
4. T.M.H. Lee, Over-the-counter biosensors: Past, present, and future, *Sensors* (2008), 8, 5535-5559.
5. A. Voller, A. Bartlett, and D.E. Bidwell, Enzyme immunoassays with special reference to ELISA techniques. *Journal of Clinical Pathology* (1978), 31, 507-520.
6. K.R. Rogers, Principles of affinity-based biosensors. *Molecular Biotechnology* (2000). 14, (2), 109-129.
7. L. Q. Gu and J. W. Shim, Single molecule sensing by nanopores and nanopore devices. *Analyst* (2009), 135, 441-451.
8. J. Clarke, H. Wu, L. Jayasinghe, A. Patel, S. Reid & H. Bayley, Continuous base identification for single-molecule nanopore DNA sequencing. *Nature Nanotechnology* (2009), 4, 265 – 270.
9. C. A. Barrios, V. Canalejas-Tejero, S. Herranz, J. Urraca, M. C. Moreno-Bondi, M. Avella-Oliver, Á. Maquieira and R. Puchades, Aluminum Nanoholes for Optical Biosensing. *Biosensors* (2015), 5, 417-431.
10. P. Hanarp, D. S Sutherland, J. Gold, B. Kasemo, Control of nanoparticle film structure for colloidal lithography. *Colloids and Surfaces A: Physicochem* (2003), 214, 23 -36.
11. M. McCord, M. Rooks, In: P. Rai-Choudhury (Ed.), Handbook of Microlithography, Micromachining, and Microfabrication. *SPIE* (1997), Chapter 2.
12. B. Ai, Y. Yu, H. Möhwald, G. Zhang, B. Yang, Plasmonic films based on colloidal lithography. *Advances in Colloid and Interface Science* (2014), 206, 5-16.
13. J. N. Anker, W. P. Hall, O. Lyandres, N. C. Shah, J. Zhao & R. P. Van Duyne, Biosensing with plasmonic nanosensors. *Nature Materials* (2008), 7, 442 – 453.
14. A. B. Dahlin, N. J. Wittenberg, F. Hook, S.-H. Oh, *nanophotonics* (2013), 2, 83.
15. S Chen, M Svedendahl, M Käll, L Gunnarsson and A Dmitriev, Ultrahigh sensitivity made simple: nanoplasmonic label-free biosensing with an extremely low limit-of-detection for bacterial and cancer diagnostics. *Nanotechnology* (2009), 20, 43.
16. G. A. Rechnitz, R. K. Kobosa, S. J. Riechela, C. R. Gebauer. A bio-selective membrane electrode prepared with living bacterial cells. *Analytica Chimica Acta* (1977), 94, 357-365.

17. J. P. Chambers, B. P. Arulanandam, L. L. Matta, W. Weis, J. J., Biosensor Recognition ElementsValdes (2008). *Biosensor Recognition Elements* (2008), 10, 1–12.
18. S. A. Maier, *Plasmonics - Fundamentals and Applications* (2007). Springer.
19. T. W. Ebbesen, H. J. Lezec, H. F. Ghaemi, T. Thio, P. A. Wolff, Extraordinary optical transmission through sub-wavelength hole arrays. *Nature* (1998), 391, 667-669.
20. Dahlin AB, Jonsson MP, Hook F, Specific self-assembly of single lipid vesicles in nanoplasmonic apertures in gold. *Adv Mater.* (2008), 20, 1436.
21. J Junesch, T, Sannomiya, A. B Dahlin, Optical Properties of Nanohole Arrays in Metal Dielectric Double Films Prepared by Mask-on-Metal Colloidal Lithography. *Acs Nano* (2012), 6, 10405–10415.
22. A. B. Dahlin, M. Mapar, K. Xiong, F. Mazzotta, F. Höök, and T. Sannomiya, Plasmonic Nanopores in Metal-Insulator-Metal Films. *Adv. Opt. Mater* (2014), 2 (6), 556–564.
23. M. Virk & K. Xiong, M. Svedendahl, M. Käll, and A.B. Dahlin, A thermal plasmonic sensor platform: Resistive heating of nanohole arrays. *Nano Letters* (2014), 14 (6), 3544-3549.
24. A. X. Wang, X. Kong, Review of Recent Progress of Plasmonic Materials and Nano-Structures for Surface-Enhanced Raman Scattering. *Materials* (2015), 8, 3024-3052.
25. M. D. Fischbein, M. Drndić, Sub-10 nm Device Fabrication in a Transmission Electron Microscope. *Nano Letters* (2007), 7 (5), 1329-1337.
26. G. Zhang, D. Wang, Colloidal lithography-the art of nanochemical patterning. *Chemistry-AnAsianJ* (2009), 4 (2), 236–245.
27. Q. Li, X. Han, J. Hou, J. Yin, S. Jiang, C. Lu. Patterning Poly (dimethylsiloxane) Microspheres via Combination of Oxygen Plasma Exposure and Solvent Treatment. *J Phys Chem B* (2015), 119, 13450–13461.
28. D. Sintona, P. Wooda, C. Escobedo, F. Eftekhari, J. Ferreirac, A. G. Broloc, R. Gordonb, Microfluidic and Nanofluidic Integration of Plasmonic Substrates for Biosensing. *Photonic Microdevices/Microstructures for Sensing* (2009), 732206.
29. A. B. Dahlin, *Plasmonic Biosensors* (2012). Amsterdam.
30. N. Jeffrey, W. Anker, H. Paige, L. Olga, C. S. Nilam, Z. Jing & P. V. Richard. Biosensing with plasmonic nanosensors. *Nature Mater* (2008), 7, 442–453.
31. K. M. Mayer, J. H. Hafner, Localized surface plasmon resonance sensors. *Chem Rev.* (2011), 111 (6), 3828-57.
32. A. R. Hawkins, H. Schmidt, Periodic nanohole arrays with shape-enhanced plasmon resonance as real-time biosensors. *Applied Physics Letters* (2010), 90.
33. R. Zia, M. D. Selker, P. B. Catrysse, and M. L. Brongersma. Geometries and materials for subwavelength surface plasmon modes, *J. Opt. Soc. Am. A* (2004), 21, 2442–2446.
34. J. M. Pitarke, V. M. Silkin, E. V. Chulkov and P M Echenique, Theory of surface plasmons and surface-plasmon polaritons. *Rep. Prog. Phys* (2007), 70, 1–87.

35. M.P. Jonsson, A.B. Dahlin, P. Jönsson, F. Höök. Nanoplasmonic biosensing with focus on short-range ordered nanoholes in thin metal films (review), *Biointerphases* (**2008**), 3 (3), 30-40.
36. P. B. Johnson, R. W. Christy, Optical-Constants of Noble-Metals. *Phys. Rev. B* (**1972**), 6, 4370–4379.
37. T. Park, N. Mirin, J. B. Lassiter, C. L. Nehl, N. J. Halas, and P. Nordlander, Optical Properties of a Nanosized Hole in a Thin Metallic Film. *ACS Nano* (**2008**), 2(1), 25-32.
38. Z. Y. Fang, Y. R. Zhen, O. Neumann, A. Polman, F. J. G. de Abajo, P. Nordlander, N. J. Halas, Evolution of Light-Induced Vapor Generation at a Liquid-Immersed Metallic Nanoparticle. *Nano Lett* (**2013**), 13 (4), 1736-1742.
39. C. Langhammer, E. M. Larsson, B. Kasemo, I. Zoric, Indirect Nanoplasmonic Sensing: Ultrasensitive Experimental Platform for Nanomaterials Science and Optical Nanocalorimetry. *Nano Lett* (**2010**), 10 (9), 3529-3538.
40. O. A. Yeshchenko, I. S. Bondarchuk, V. S. Gurin, I. M. Dmitruk, A. V. Kotko, *Surf Sci* (**2013**), 608, 275-281.
41. C. Vericat, M. E. Vela, G. Benitez, P. Carro, R. C. Salvarezza, Self-assembled monolayers of thiols and dithiols on gold: new challenges for a well-known system. *Chem Soc Rev* (**2010**), 39 (5), 1805-1834.
42. S. Fatima, R. H. Khan, Effect of Polyethylene Glycols on the Function and Structure of Thiol Proteases. *J. Biochem* (**2007**), 142, 65–72.
43. A. Hebeish, S. Farag, S. Sharaf, T.I. Shaheen, Thermal responsive hydrogels Based on semi interpenetrating network of poly (NIPAm) and cellulose nanowhiskers, *Carbohydrate Polymers* (**2013**), 102, 159–166.
44. R. S. Pytel, E. Thomas, I. Hunter, Anisotropy of electroactive strain in highly stretched polypyrrole actuators, *Chem Mater* (**2006**), 18, 861.
45. J. Junesch, G. Emilsson & K. Xiong, S. Kumar, T. Sannomiya, H. Pace, J. Vörös, S.-H. Oh, M. Bally, A.B. Dahlin, Location-specific nanoplasmonic sensing of biomolecular binding to lipid membranes with negative curvature. *Nanoscale* (**2015**), 7 (37), 15080-15085.
46. P. Hanarp, D. S. Sutherland, J. Gold and B. Kasemo, Colloids and Surfaces A: Physicochemical and Engineering Aspects, **2003**, 214, 23-36.
47. E. Stefan Kooij, Bene Poelsema, Shape and size effects in the optical properties of metallic nanorods. *Phys. Chem. Chem. Phys* (**2006**), 8, 3349–3357.
48. T. H. Reilly, R. C. Tenent, T. M. Barnes, K. L. Rowlen, J. v. d. Lagemaat, Controlling the Optical Properties of Plasmonic Disordered Nanohole Silver Films. *ACS Nano* (**2010**), 4 (2), 615-624.
49. O.A. Yeshchenko, I. S. Bondarchuk, V. S. Gurin, I. M. Dmitruk, A.V. Kotko, Temperature dependence of the surface plasmon resonance in gold nanoparticles. *Surface Science* (**2013**), 608, 275–281.
50. F. Avilés, O. Ceh , A. I. Oliva, Physical properties of Au and Al thin films measured by resistive heating. *Surface Review and Letters* (**2005**), 12, 101-106.

51. R. Kekesi, D. Meneses-Rodriguez, F. Garcia-Perez, M. U. Gonzalez, A. Garcia-Martín, A. Cebollada and G. Armelles, The effect of holes in the dispersion relation of propagative surface plasmon modes of nanoperforated semitransparent metallic films. *Journal of Applied Physics* (2014), 116, 134306.

## **A Thermal Plasmonic Sensor Platform: Resistive Heating of Nanohole Arrays**

Mudassar Virk & Kunli Xiong, Mikael Svedendahl, Mikael Kall, and Andreas B. Dahlin\*\*

Department of Applied Physics, Chalmers University of Technology, Göteborg, Sweden

Corresponding Author

\*E-mail:

[adahlin@chalmers.se](mailto:adahlin@chalmers.se).

*Nano Lett.* **2014**, 14, 3544–3549

